USGS
science for a changing world

Prepared for the National Aeronautics and Space Administration

Geologic Map of the Source Region of Shalbatana Vallis, Mars

By Daniel C. Berman, J. Alexis Palmero Rodriguez, Catherine M. Weitz, and David A. Crown

Pamphlet to accompany
Scientific Investigations Map 3492

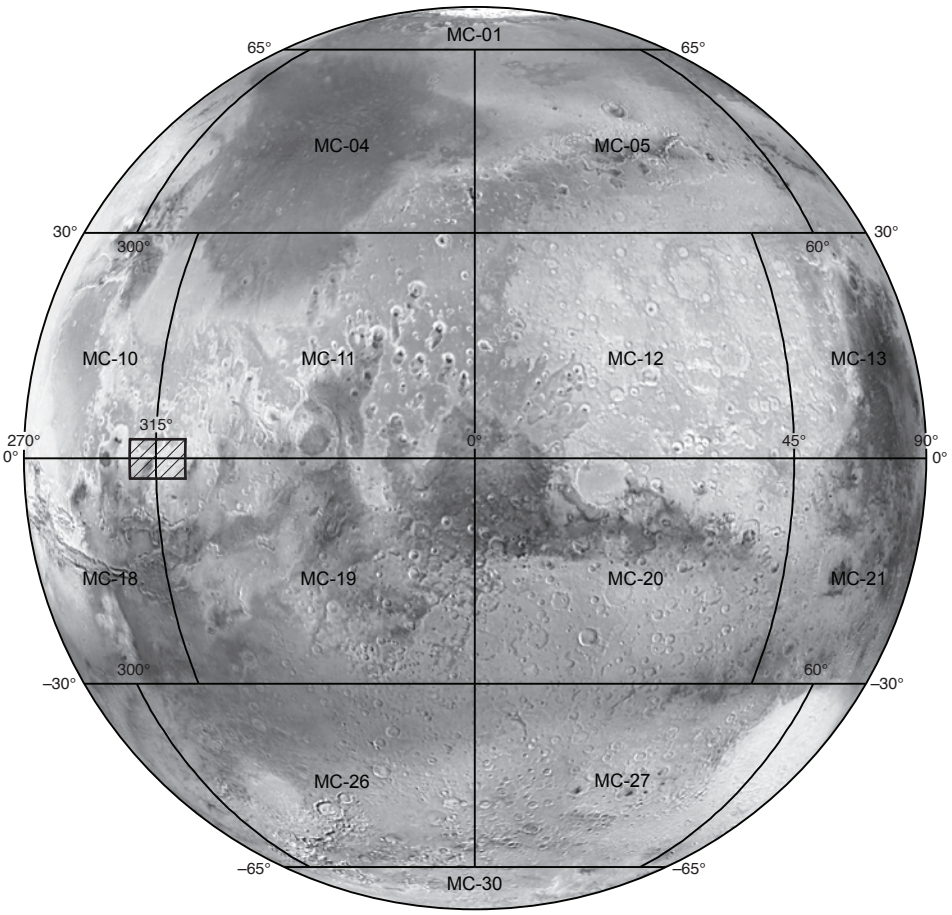

2023

U.S. Department of the Interior
U.S. Geological Survey

U.S. Geological Survey, Reston, Virginia: 2023

Suggested citation:
Berman, D.C., Rodriguez, J.A.P., Weitz, C.M., and Crown, D.A., 2023, Geologic map of the source region of Shalbatana Vallis, Mars: U.S. Geological Survey Scientific Investigations Map 3492, pamphlet 10 p., scale 1:750,000, https://doi.org/10.3133/sim3492.

ISSN 2329-1311 (print)
ISSN 2329-132X (online)

Cover. Photomosaic showing location of map area (hachured rectangle). An outline of 1:5,000,000-scale Mars Chart quandrangles is provided for reference.

Contents

Figures

Table

Geologic Map of the Source Region of Shalbatana Vallis, Mars

By Daniel C. Berman,[1] J. Alexis Palmero Rodriguez,[1] Catherine M. Weitz,[1] and David A. Crown[1]

Introduction

Xanthe Terra is a high-standing cratered plain located southeast of Lunae Planum and south of Chryse Planitia in the western equatorial region of Mars (fig. 1, map sheet). It contains landforms shaped by diverse geologic processes, including various scales of channels and valleys, chaotic terrains, delta-fan deposits, and landslides. Xanthe Terra contains impact craters of a wide range of sizes and degradation states. Some craters exhibit well-preserved lobate ejecta deposits and others are almost completely buried or eroded. Some craters are infilled by deposits that have undergone fracturing.

A thoroughly investigated, extensive outflow system is located within Xanthe Terra and the surrounding circum-Chryse Planitia, including Shalbatana, Ravi, Ares, Kasei, Mawrth, Simud, and Tiu Valles (for example, McCauley and others, 1972; Sharp, 1973; Tanaka and others, 2014). The formation of outflow channels has been attributed to various mechanisms, including erosion by catastrophic floods (Baker and others, 1991), glaciers (Lucchitta, 1998, 2001; Chapman and Kargel, 1999), debris flows (Golombek and others, 1997; Nummedal and Prior, 1981; Tanaka, 1999; Rodriguez and others, 2006a,b), and (or) lava flows (Leverington, 2011, 2019a,b; Hopper and Leverington, 2014). The catastrophic flood hypothesis suggests that the history of the channel was dominated by catastrophic floods generated by groundwater outbursts (for example, Carr, 1979; Clifford, 1993; Clifford and Parker, 2001) and that, in turn, collapse over evacuated aquifer sections produced vast areas of ruptured crust known as chaotic terrain (for example, McCauley and others, 1972; Sharp, 1973; Baker and Milton, 1974; Scott and Carr, 1978; Lucchitta, 1982, 2001; Scott and Tanaka, 1986; Baker and others, 1991). This manner of collapse would result in chaotic terrain forming simultaneously, or shortly after, the groundwater outbursts and aquifer evacuation. The floods were likely episodic during the Hesperian and Amazonian Periods as the Martian climate transitioned from warmer and wetter to colder and drier (Pacifici, 2008; Warner and others, 2010, 2011, 2013a; Rodriguez and others, 2011, 2014, 2015a,b; Roda and others, 2014), with likely peaks in activity during the Late Hesperian (Rotto and Tanaka, 1995; Tanaka and others, 2014) and Middle Amazonian (Rodriguez and others, 2014, 2015a,b).

Shalbatana Vallis, the outflow channel at the focus of this mapping effort, extends northeast from the ~120 km diameter Orson Welles crater, which contains extensive chaotic terrain units on its floor. These, along with Aromatum Chaos, Ravi Vallis, and surrounding fractured crater fill, indicate a history of prominent topographic modification due to collapse and subsidence from hundreds of meters to several kilometers. Shalbatana Vallis is thought to have been active over a prolonged time period, extending from the Hesperian to the Early Amazonian (Scott and Tanaka, 1986; Rotto and Tanaka, 1995; Nelson and Greeley, 1999; Clifford and Parker 2001; Tanaka and others, 2014). Shalbatana Vallis is unique among the circum-Chryse Planitia outflow channels because it does not connect upstream to the other outflow channels and, although it attains similar depth ranges to other circum-Chryse Planitia outflow channels (~2 km), it is considerably narrower (~15 km wide) (see figs. 1 and 2, map sheet). It also exhibits relatively fewer erosional bedforms. Furthermore, while collapsed highlands (in other words, chaotic terrain) form the source regions of most of the southern circum-Chryse Planitia outflow channels, Shalbatana Vallis extends from the collapsed floor of a large impact crater. The shape of its channels may imply a different stage in outflow-channel development or excavation into different geologic materials, making the geology and evolution of surrounding Xanthe Terra important for broader interpretations of outflow-channel development, as well as for the geologic history of the Xanthe Terra region. Shalbatana Vallis includes landforms indicative of catastrophic flooding, interior lakes, and potential deltas (Di Achille and others, 2006; Hauber and others, 2009, 2013; Goudge and others, 2012), illustrating its hydrogeologic significance.

Xanthe Terra is also dissected by Noachian to Early Hesperian valley networks that incise the intercrater plains. These valleys are much narrower (~1 km wide) and shallower (tens of meters in depth) than the regional outflow channels, and their formation has been attributed to fluvial dissection from rainfall or snow melt (Carr, 1981; Carr and Malin, 2000; Baker, 2001; Hauber and others, 2009). In addition, a series of deeply incised valleys (several hundred meters in depth and ~3–5 km wide) are morphologically distinct from the small, shallow network valleys that incise Xanthe Terra. These systems include Nanedi, Hypanis, Sabrina, Ochus, Drilon, and Subur Valles. These deeper valleys have amphitheater

[1]Planetary Science Institute

heads, low drainage densities, few tributaries, and nearly constant widths—characteristics that are generally consistent with the interpretation that they were formed by groundwater sapping (Pieri, 1976; Squyres, 1989; Carr, 1996; Carr and Malin, 2000; Baker, 2001; Hauber and others, 2009). Nanedi Valles was determined to be Hesperian by Scott and Tanaka (1986) and Crumpler (1997) and Noachian to Hesperian by Rotto and Tanaka (1995). Both Sabrina and Hypanis Valles terminate in large delta-like deposits along the boundary of Chryse Planitia (Hauber and others, 2009, 2013; Adler and others, 2018; Fawdon and others, 2018). The Hypanis Valles fan was identified as a possible landing site for the ExoMars 2018 (Fawdon and others, 2018) and Mars 2020 (Adler and others, 2018) landers because the fan provides evidence for subaqueous sediment deposition that would preserve possible biosignatures.

Short, sinuous channels extend into multiple craters within Xanthe Terra. Several of these terminate in fan deposits as they breach crater walls and debouch onto their floors. These fans have been interpreted as both delta fans formed in paleolakes within craters and as alluvial fans (Di Achille and others, 2006; Hauber and others, 2009, 2013; Goudge and others, 2012). Di Achille and others (2007) mapped a small portion of central Shalbatana Vallis and found evidence for a paleolake on the channel floor. Numerous studies have identified a multitude of craters in the Xanthe Terra region as potential paleolake basins (for example, Cabrol and Grin, 1999, 2001; Di Achille and others, 2006; Hauber and others, 2009, 2013; Goudge and others, 2012) and many contain possible deltaic features (Howard and others, 2005; Irwin and others, 2005; Moore and Howard, 2005; Di Achille and Hynek, 2010).

An elongate depression (~55 km in width, ~300 km in length, as much as ~3 km in depth) extends north from Ganges Chasma to Orson Welles crater (fig. 3, map sheet); the northern portion of the depression is in the southern map area. This depression has been interpreted as having formed due to surface collapse and subsidence that resulted from subterranean erosion by water that flowed from Ganges Chasma to form Shalbatana and Ravi Valles (Carr, 1995; Cabrol and others, 1995, 1997) and (or) as water that was extracted from an ice-rich, multi-kilometer-deep cryosphere through magmatic heating and released to form the outflow channels (Rodriguez and others, 2003). A shallower branch of this depression (~1 km in depth) extends northeast to Aromatum Chaos and includes a deeper depression ~1.8 km deep. These depressions contain a multitude of structural features such as faults and troughs (described in detail below).

The region for this geologic map has not been mapped with post-Viking Orbiter datasets at a scale greater than 1:20,000,000. Previous mapping at a smaller scale (Scott and Tanaka, 1986; Rotto and Tanaka, 1995) was mainly based on Viking Orbiter datasets at resolutions of greater than 150 m/pixel, with some higher resolution images (~60 m/pixel) over portions of Aromatum Chaos and Ravi Vallis. The 2014 global geologic map of Mars (Tanaka and others, 2014) used higher resolution datasets but was at a scale of 1:20,000,000. Currently available datasets provide substantial new information to identify and describe geologic units, analyze morphology and spectra, and assess geologic relations. Recent, high-resolution datasets reveal a potentially more complex history of flooding and collapse than previously observed. Geologic mapping at a scale of 1:750,000 using these datasets allowed us to characterize and summarize this history in greater detail.

Geography

The study region within Xanthe Terra is defined by Mars Transverse Mercator (MTM) 00042 and 00047 quadrangles (lat 2.5° N. to −2.5° N., long 310° to 320° E.) and includes Orson Welles crater (124.5 km diameter, the source region for Shalbatana Vallis), the southernmost portion of Shalbatana Vallis, Aromatum Chaos (the source region for Ravi Vallis), the westernmost portion of Ravi Vallis, and the source area of Nanedi Valles. Iamuna Chaos is located on the etched floor of Ravi Vallis. In addition to Orson Welles crater, the study region includes the craters Dia-Cau (29.7 km), Rypin (18.4 km), Windfall (17.9 km), and Žulanka (47.1 km) and the westernmost portions of craters Chimbote (67.2 km) and Da Vinci (100.2 km). Other large, rimless, flat-floored craters (ranging in size from ~10 km to ~50 km in diameter), some with floor fractures (mapped by Rotto and Tanaka, 1995, as Amazonian/Hesperian chaotic material), are also found in the study region. These floor-fractured craters are interpreted to have formed due to the collapse of subsurface aquifers (Sato and others, 2010) or ice-covered lakes (Roda and others, 2014). The study region also includes the northernmost portion of the depression south and southeast of Orson Welles crater, as well as various collapse pits within the depression.

Published geologic maps of the study region include 1:5,000,000-scale maps based on Mariner 9 data (Wilhelms, 1976; Saunders, 1979), the Viking-based map produced by Rotto and Tanaka (1995) at a 1:5,000,000 scale, the northern plains map that has scales ranging from 1:15,000,000 at the north pole to 1:7,500,000 at the equator and that was produced using Mars Global Surveyor (MGS) Mars Orbiter Laser Altimeter (MOLA) and Mars Orbiter Camera (MOC) data (Tanaka and others, 2005), and the 2014 global geologic map of Mars (Tanaka and others, 2014) at 1:20,000,000 scale using primarily MGS MOLA and Odyssey Thermal Emission Image System (THEMIS) infrared (IR) data. These previously published maps provide context to our mapping. Other previous studies also provide mapping and reconstructions of outflow-channel extents and the history of this region (Greeley and others, 1977; Tanaka, 1997, 1999). The Rotto and Tanaka (1995) map is the most detailed and comprehensive existing map of the region. Their map portrays a generalized geologic history, in which chaotic terrains and outflow channels mostly developed between the Late Hesperian and the Early Amazonian.

Prior investigations have suggested that the geologic evolution of Xanthe Terra spans a large portion of the history of Mars. Mapping by both Scott and Tanaka (1986) and Rotto and Tanaka (1995) suggests that the outflow channels in general formed during the Late Hesperian/Early Amazonian. Due to the limited image resolution available, the wall materials of these outflow channels were mapped primarily as stratigraphically undivided materials (Scott and Tanaka, 1986), locally covered by materials associated with zones of prominent wall retreat (Rotto and Tanaka, 1995).

Rotto and Tanaka (1995) recognized two distinct outflow-channel types within their map area. The higher outflow channels are incised at various levels on the highlands and consist of ~20 to ~50-km-wide canyons, the floors of which are marked by prominent ridges and grooves. The lower outflow channels form the deepest levels of flow dissection. These lower outflow

channels consist of much broader valleys, generally a few hundred kilometers in width; their floors are largely depositional, lacking well-developed bedforms. Rodriguez and others (2006a) proposed that the higher channels were produced by floods sourced regionally within the circum-Chryse Planitia highlands, whereas the lower floors formed by debris-flow discharges, which likely were released from collapse in the eastern chasmata. In addition, the possible occurrence of volcanic landforms and indications of regional glaciation on the floor of Valles Marineris (Gourronc and others, 2014) may have promoted volcano-ice interactions that generated megafloods, which extended through the lower channel floors. Possible sites of megaflood discharges have been documented in central (Lucchitta and others, 1994; Rotto and Tanaka, 1995) and eastern (Warner and others, 2013b) Valles Marineris. The interior of southern circum-Chryse Planitia includes a system of lower outflow-channel floors that form an enclosed basin, which might include submarine sedimentation following Late Hesperian catastrophic floods from Valles Marineris (Rodriguez and others, 2019).

Scott and Tanaka (1986) and Rotto and Tanaka (1995) identified two primary plains units within the study region: the Middle Noachian cratered unit Npl1 and the relatively smooth subdued cratered unit Npl2. These units were interpreted to consist of brecciated lavas from the Middle Noachian that were resurfaced in the Late Noachian, leaving relatively smooth plains materials, eolian materials, and fluvial deposits. A hilly Noachian plains unit (Scott and Tanaka, 1986; Rotto and Tanaka, 1995; Crumpler, 1997) was also identified on the northwest margin of Xanthe Terra that may be similar to the Noachian knobby unit that we identified in our map area. Crumpler (1997) interpreted this unit as remnants of the more widespread hummocky highland material that has been eroded and almost completely removed.

The 2014 global geologic map (Tanaka and others, 2014) identified a Middle Noachian highland unit equivalent to units Npl1 and Npl2 and an Early Noachian highland unit roughly equivalent to the hilly plains described above. They also mapped chaotic terrains as a single Hesperian transition unit.

Base Map and Data

The Mars Odyssey THEMIS IR daytime mosaic (100 m/pixel) was used as the primary base map. Supplementary image and topographic datasets used to assist in identification of unit boundaries and superposition relations included (1) the THEMIS nighttime IR mosaic (100 m/pixel); (2) Mars Reconnaissance Orbiter (MRO) Context Camera (CTX) images (~5–6 m/pixel; CTX coverage of the map area is complete at ~6 m/pixel resolution); (3) the Mars Global Surveyor MOLA Mission Experiment Gridded Data Records (MEGDR; ~462 m/pixel); and (4) Mars Express (MEX) High Resolution Stereo Camera (HRSC) nadir images (color, stereo at >12 m/pixel) and Digital Elevation Models (DEMs, constructed from stereo nadir images). HRSC coverage of the map area is nearly complete with 12.5 and (or) 25 m/pixel image mosaics and a DEM mosaic at 100 m/pixel in resolution. Supplementary image datasets were used to help discern geologic unit boundaries, to identify feature type, and to measure crater diameters. Topographic datasets were used to analyze superposition and embayment relations between geologic units (for example, fig. 4, map sheet).

All images not provided by the U.S. Geological Survey (USGS), including CTX, High Resolution Imaging Science Experiment (HiRISE), and HRSC, were processed with Integrated Software for Imagers and Spectrometers (ISIS; http://isis.astrogeology.usgs.gov) from raw format to geometrically calibrated, noise-reduced, map-projected images. Images were then imported into geographic information system (GIS) software for georeferencing, display, and analysis.

Methodology

We constructed the geologic map of the source region of Shalbatana Vallis at 1:750,000 scale according to the methods described by Tanaka and others (2005) and Skinner and others (2022). Below, we describe (1) digital drafting parameters used to compile information, (2) unit groups, names, symbols, and definitions, (3) types of geologic contacts, and (4) types of feature symbols. These, in combination with the Description of Map Units (see map sheet), show our methodology for constructing the final map product.

Digital Drafting Parameters

We digitized contact, line, and polygon features using a GIS at a scale of approximately 1:150,000 to 1:200,000 (4–5 times the publication map scale of 1:750,000). We manually digitized lines at ~300–400 m intervals. We did not use GIS streaming capabilities for this product.

Unit Groups, Names, Labels, and Definitions

We grouped geologic units into geomorphic categories rather than geographic provinces (for example, Skinner and others, 2022), because the map area exists within a single province. We selected geomorphic categories for geologic units on the basis of similarity of primary unit characteristics. Therein, we defined 16 geologic units in the map area, which we divided into the following groups: plains units, channel units, crater units, chaos units, flow units, and surficial units.

We assigned unit names on the basis of their general geomorphological characteristics (consistent with previous usage when possible), as well as stratigraphic position (for example, channel material, higher smooth and channel material, lower etched). We mapped the ejecta blanket for Orson Welles crater separately from other crater materials, because it is one of the largest features on the map.

We assigned each mapped unit a label that uniquely identifies the chronologic period(s) in capital form (for example, N = Noachian Period). Units such as Npl and HcOW are mapped so that they meet wall rock units at the upper scarp margins; we recognize they do not have zero thickness in true geologic terms, and these materials are included to some degree in unit HNu. Given

the map scale and base-map resolution, we drew contacts at the margin between the surface and the walls. We mapped units based on a combination of geomorphology, topography, and stratigraphic relations. For complete descriptions and interpretations of the map units, see the Description of Map Units (map sheet).

Contact Types

We attributed contact types as either certain or approximate. We delineated certain contacts when unit contacts were clearly discernable on the base map or in supplementary datasets. We delineated approximate contacts where the exact locations of unit contacts were more difficult to assess or when units thinned gradually at their farthest extents, such as crater ejecta blankets.

Feature Types

Mapped linear features include ridge crests, scarp crests, channels, crests of crater rims, crests of buried or degraded crater rims, graben traces, grooves, troughs, and faults. Surface features include secondary crater chains and dark ejecta material. These are described in more detail below.

Mapped Features

Ridges

We identified one type of positive-relief ridge feature in the map area. A ridge crest denotes the crest of a linear to curvilinear ridge; ridges are found throughout the map area, but occur primarily on the cratered plains unit (Npl). These features generally have a north-south orientation. The vast majority of these, particularly the north-south-oriented ridges, are crenulated and interpreted as wrinkle ridges, consistent with those found in the greater Xanthe and Lunae Planum regions (Scott and Tanaka, 1986; Tanaka and others, 2014). Channel-parallel, east-west-oriented ridges along the margin of the northern upper floor (unit AHchhs) of Ravi Vallis are noncrenulated. Ridges southwest of Aromatum Chaos are sharp crested and symmetric. We mapped 102 ridge crests within the map area, ranging in length from 2.4 km to 50.5 km (13.1 km mean). We used HRSC DEM data to create elevation profiles for 10 wrinkle-type ridges and they ranged in height from 25 m to 100 m, with a mean of 59 m. The large ridge bounding the north of Ravi Vallis is about 80 m in height. The sharp-crested ridges southwest of Aromatum Chaos are about 90 m in height.

Scarps

A scarp crest is a linear to curvilinear sharp topographic boundary at the margins of collapsed or eroded terrains where material was removed (unlike a fault where a surface has dropped down). We mapped 87 scarp crests ranging in length from 1.8 km to 36.5 km with a mean of 12.9 km and ranging in depths from ~250 m to 1,500 m along collapsed/eroded terrains and from ~65 m to 280 m in Ravi Vallis.

Faults

A normal fault is a topographic offset where one side of the terrain has dropped, with the slope face angled toward the higher side, for example the two inward-facing faults bounding a graben. In some places, we mapped a series of cascading faults facing the same direction in a stair-step-like pattern. We mapped 39 normal faults, ranging in length from 1.4 km to 18.7 km (mean 8.1) and ranging in depth from ~120 m to ~250 m.

Linear to Curvilinear Depressions

We mapped three types of linear to curvilinear depressions in the map area. A trough is a linear to curvilinear depression found both within crater fill material (unit Hf) and within the elongated depression extending from the south of Orson Welles crater to Aromatum Chaos. Many troughs are composed of a series of interconnected pits. They are also found in the higher smooth-channel deposits where plains materials have collapsed along Shalbatana Vallis just before it begins to narrow. They appear to be formed by collapse, subsidence, and (or) structural deformation of the surface materials. We mapped 206 troughs ranging in length from 1.4 km to 34.6 km with a mean of 7.8 km. We measured the depths of 10 troughs and they ranged from ~60 m to ~190 m, with a mean of 113 m.

A graben trace marks the location of a linear to curvilinear flat-floored depression, bounded by two inward-facing normal faults, that is too small for its faults to be mapped at the map scale (in other words, less than ~1 km apart). We mapped 36 graben traces ranging in length from 1.6 km to 16.0 km, with a mean of 7.7 km, and ranging in depth from ~40 m to ~60 m.

A channel is a narrow, sinuous to branching shallow depression. Most are interpreted to have formed by fluvial incision. Examples include the small channels entering Nanedi Valles and descending the walls of Orson Welles crater. We mapped 94 channels ranging in length from 315 m to 32.4 km, with a mean of 7.0 km.

Crater Rims

We mapped crater rims for all craters 4 km and larger in diameter (this size was chosen based on the print scale of the map). We identified two types of crater rims. A crest of crater rim indicates an impact crater rim that clearly rises above the surrounding terrain. We mapped 100 crater-rim-crest segments. A crest of buried or degraded crater rim is an inferred crater rim that has been degraded or buried, so it does not have a visibly raised edge but a circular outline is still visible. We mapped 31 buried or degraded crater-rim-crest segments. We did not map these where a geologic contact was drawn along the rim crest or degraded rim.

Surface Features

A secondary crater chain is a linear chain of craters that formed by secondary impacts from a larger impact crater. Most of these are in discontinuous chains that emanate radially from

Orson Welles crater and are subcircular in planform and shallow, indicating low velocity impacts. As distance from Orson Welles crater increases, the crater margins become less distinct and the craters become gradually shallower.

We mapped dark ejecta material around craters that had ejecta deposits that were distinctly darker than the surrounding terrain in the THEMIS daytime IR basemap and (or) brighter in the THEMIS nighttime IR mosaic. These materials were excavated from depth and deposited on the surrounding terrain, so they are likely a different composition from the underlying surface.

Age Determinations

We measured and catalogued crater diameters using the three-point GIS tool CraterTools (Kneissl and others, 2011), using CTX images, because the higher resolution provided more accurate results and the areal coverage was complete. Unit areas, crater densities, crater-density ages, and superposition relations with contiguous units are presented in table 1. We did not count crater units individually, with the exception of Orson Welles and Dia-Cau craters, because they are generally too small for reliable statistical results. To calculate ages of geologic units, we combined superposing craters and their areas with the units they superposed. We removed areas of secondary crater clusters for the purposes of crater counting.

We calculated cumulative densities of craters greater than or equal to 1, 2, 5, and 16 kilometers per unit area normalized to 1,000,000 km^2 (N(1), N(2), N(5), and N(16), respectively, table 1). We also derived model absolute ages for all units where possible, including for smaller units that did not contain craters 1 km in diameter or larger (such as unit Alf), using size-frequency distributions using the production function of Hartmann (2005) and the chronology function of Hartmann (2005) as updated by Michael (2013). We used these values, in combination with cross-cutting and stratigraphic relations, to assign map units to the eight Martian epochs on the basis of the scheme of Tanaka (1986) as updated by Michael (2013).

For most units where craters greater than 1 km in diameter were available (except for unit Npl), we derived unit ages from N(1) populations on the basis of the statistical robustness of those ages and given the relatively small unit areas. For unit Npl, we assigned a Late Noachian age based on the N(2) age, because this was most consistent with superposition relations and the model absolute age. When assigning ages, we gave cumultative N ages the most weight over absolute model ages. When those ages did not agree with stratigraphic relations, we took model ages from size-frequency distributions into account. If discrepancies still existed, we used stratigraphic relations and referenced work to make age assumptions. For example, unit AHcth had a younger N(1) age and absolute model age than AHctl; however, stratigraphic relations suggest the opposite is the case. It is likely that the small areal extent of unit AHcth, in combination with the many sloped surfaces and mass wasting materials, obscure its true age, so we assigned its age as Late Hesperian–Early Amazonian and positioned it accordingly on the Correlation of Map Units (map sheet). In addition, N(1) counts for unit AHchhs did not extend into the Amazonian; however, the model absolute age and superposition relations suggested an age of Late Hesperian–Early Amazonian.

Units without crater counts are assigned ages based on assumptions, stratigraphic relations, and previous work. For example, undivided wall material is traditionally assigned unit label "HNu," because it is a combination of Noachian basement rock and superposed surficial deposits that formed through the Hesperian (and in some cases, for example in relation to unit Alf, into the Amazonian). Crater units are traditionally assigned the unit label "AHc," because older crater materials are mostly eroded. Knobby material is too small for crater counts, but it is stratigraphically the oldest unit and likely formed in the Early Noachian. For ages of other units, see table 1.

Geologic Summary

We summarize the geologic history of the source region of Shalbatana Vallis in Xanthe Terra, Mars, on the basis of the geologic unit and feature mapping and stratigraphic determinations presented herein. This summary is portrayed graphically in the accompanying Correlation of Map Units (map sheet).

Noachian Period

During the Early to Middle Noachian Epochs, ancient highland materials in the Xanthe Terra region, including lava and any ancient sedimentary units present, were reworked by impacts during the heavy bombardment, in particular the impact that formed the Chryse Planitia (Rotto and Tanaka, 1995; Crumpler, 1997). Remnants of these highland materials are found in the map area and are mapped as knobby materials (unit Nk). These materials underwent enhanced erosion during this period (Rotto and Tanaka, 1995).

Most of Xanthe Terra underwent widespread resurfacing during the Middle to Late Noachian, likely as a combination of lava flows, reworked crater materials, and sedimentary deposits (Rotto and Tanaka, 1995) resulting in the flat-lying, smooth plains (unit Npl) found in the map area. While previous maps (for example, Scott and Tanaka, 1986; Rotto and Tanaka, 1995) mapped two Noachian plains units in this region, we mapped only one because of the lack of consistent evidence for subdivision.

Some of the surface modification likely resulted from fluvial activity, including the initial formation of small valley networks formed by rainfall, snow melt, and larger sapping valleys (unit HNv) such as Nanedi Valles (Carr, 1996). Buffered crater counts (for example, Fassett and Head, 2008) show an upper boundary for the age of Nanedi Valles to be ~3.6 Ga in the Late Noachian to Early Hesperian, but precise age constraints are difficult to determine because of the small area of the channel floor and lack of superposed craters.

Resurfacing during this period was accompanied by erosion of the rims and removal of the ejecta blankets of craters in the region; impact craters continued to form on the plains throughout the Noachian Period and into the present as evidenced by the range of degradational morphologies of the superposed craters. Resurfacing continued into the Hesperian Period, although potentially at a lower rate.

Table 1. Characteristics of geologic units in the source region of Shalbatana Vallis, Mars: areas, crater densities, and superposition relations. Ages derived from N(1) ages except where noted.

[Ga, giga-annum; --, no data available]

Unit label	Unit name	Unit area (count area[1]) km^2	N(1)	N(2)	N(5)	N(16)	Designated age[2]	Model absolute age (Ga)	Superposition relations[3]
Ad	Dune material	823.3	2,429.2±1,717.7	--	--	--	EA–LA	1.6±1	<Al, AHchls, AHctl, HNu, AHcth
AHfa	Fan material	4.8	--	--	--	--	LH–MA[4]	--	<Hf, HNu
HNu	Wall material, undivided	8,676.4	--	--	--	--	MN–LH[4]	--	<Npl, Nk, HcOW, Hf; HNv, AHchhs, AHc, AHchls, AHctl, Alf, AHchle; >Al, Afa, Ad, HcOW, Hf, HNv, AHchhs, AHc, AHctl, AHchls, Alf, AHchle
Al	Landslide material	955.8	1,046.2±1,046.2	--	--	--	EA–LA	0.77±0.09	>Ad; <AHchls, AHcth, AHctl, AHchle, AHchhs, HNu
Alf	Lobate flow material	854.2 (648.3)	--	--	--	--	EA[4]	1.8±–0.08	<Npl, AHchhs, AHc, Hf, HNu; >HNu
AHctl	Chaotic terrain material, lower	6,136	1,792.7±540.5	977.8±399.2	163±163	--	LH–EA	1.1±0.2	>Ad, AHc, Al, HNu; ~AHchls, AHchle; <HNu
AHcth	Chaotic terrain material, higher	3,184.8	628.0±444.1	--	--	--	LH–EA[4]	0.5±0.1	>AHctl, AHchls, Al, Ad; ~AHchle; <Hf
Hf	Fill material	11,554.2 (10,583.1)	2,929.2±526.1	661.4±250	--	--	EH–LH	3.5+0.06/–0.010	<AHcth, AHctl, HNu, AHc, Npl; ~HcOW; >Afa, Alf, HNu
AHc	Crater material	4,677	--	--	--	--	EH–LA[4]	--	<Npl, HcOW; ~HNu; >AHchls, AHctl, AHchhs
HcOW	Orson Welles crater material	56,785.7 (55,194.2)	2,989.5±232.7	797.2±120.2	144.9±51.2	18.1±18.1	EH–LH	3.5+0.04/–0.05	>AHchhs, HNu, AHc, AHchls; <Npl, Nk, HNu; ~Hf
AHchls	Channel material, lower smooth	4,080.8	1,715.4±648.3	735.2±424.4	490.1±346.6	--	LH–EA	2.7+0.5/–0.7	>Ad, Al, HNu; <AHctl, AHcth, AHchhs, HcOW, HNu; ~AHchle
AHchle	Channel material, lower etched	3,693.9	2,165.7±765.7	270.7±270.7	--	--	LH–EA	3.1+0.2/–0.3	>AHchls, HNu; <AHctl, HNu, Npl, AHchhs
AHchhs	Channel material, higher smooth	14,474.8 (13,343.2)	3,147.7±485.7	1,049.2±280.4	299.8±149.9	74.9±74.9	LH–EA[4]	3.2+0.1/–0.3	>HNu, AHchls, Alf, Al, AHchle; <HcOW, AHc, HNu, Npl
HNv	Valley floor material	322.7	--	--	--	--	MN–LH[4]	--	<Npl, HNu; ~AHchhs; >HNu
Npl	Cratered plains	56,788 (62,112.7)	5,345.1±293.4	1,288±144	241.5±62.4	16.1±16.1	MN–LN[4]	3.6±0.02	~HNu; >HNu, HcOW, AHc, AHchhs, Alf, HNv; <Nk
Nk	Knobby material	216	--	--	--	--	EN–MN[4]	--	>Npl, HcOW, AHc, HNu

[1]Count area represents unit area combined with overlying impact crater units and (or) minus areas of secondary clusters, if different from unit area. See pamphlet for details.

[2]Indicates age derived from N(2) age. EA, Early Amazonian; EH, Early Hesperian; EN, Early Noachian; LA, Late Amazonian; LH, Late Hesperian; LN, Late Noachian; MA, Middle Amazonian; MN, Middle Noachian.

[3]<, younger than; ~, overlaps in time with; >, older than. Only contiguous units listed. Note that unit superposition relations between units can differ between different exposures and thus be listed as both older and younger. Undivided units, such as unit HNu, can be both older and younger than adjacent units, because they contain a mixture of older basement rock and younger talus.

[4]Indicates age derived from superposition relations, absolute model ages, and (or) referenced work.

The Noachian plains are characterized by north-south-oriented wrinkle ridges that are found throughout Xanthe Terra and Lunae Planum to the west (Scott and Tanaka, 1986; Rotto and Tanaka, 1995; Tanaka and others, 2014). These are likely related to lithologic stresses due to the rise of the Tharsis volcanic province (northwest of map area) during the Late Noachian to Early Hesperian (Tanaka and others, 2014).

Hesperian Period

Orson Welles crater (unit HcOW) was formed by a large impact during the Early to Late Hesperian. This impact may have weakened the upper crust beneath and around the crater, providing a preferred pathway for subsurface water from Ganges Chasma north toward Chryse Planitia and east toward Hydraotes Chaos, initiating the subsidence and collapse along this pathway. The Orson Welles impact may also have led to the initial collapse of the depression that contains Aromatum Chaos. We mapped the ejecta of Orson Welles to a much larger extent than previous maps, because it gradually thins and the outer deposits are only visible at the higher resolution used in our mapping.

Erosion in the plains throughout the Hesperian led to the degradation of the Orson Welles crater rim. Other large craters in the map area likely formed during the Early Hesperian, including Dia-Cau crater (model age ~3.4–3.6 Ga). The ejecta of Dia-Cau is crosscut by Ravi Vallis; therefore, much of the activity that formed the channel (and Aromatum Chaos) occurred after the Dia-Cau impact. Model ages indicate that incision began shortly after impact and continued into the Hesperian (see table 1).

During the Hesperian, many depressions in the map area were infilled with smooth materials (unit Hf, Early to Late Hesperian), including large craters such as Orson Welles and potentially the collapse depression containing Aromatum Chaos and Iamuna Chaos. Unit HcOW materials may superpose some of the craters with unit Hf deposits on their floors; however, the relations are not entirely clear given the thin and discontinuous nature of ejecta deposits and subsequent effects of erosion, which indicates that this infilling may have occurred over a long period of time.

Our observations of high-standing smooth flood deposits (unit AHchhs) surrounding Orson Welles crater and Aromatum Chaos (not previously mapped by others) suggest that paleolakes formed in both of these depressions during the Late Hesperian and, at some time, overflowed the tops of the depressions. While Rotto and Tanaka (1995) mapped the entire region between Ganges Chasma and Orson Welles crater as higher-channel deposits, we mapped Orson Welles ejecta deposits surrounding an exposure of higher-channel deposits extending from the southernmost depression in the map area. These overflow deposits embay the Orson Welles ejecta, Dia-Cau ejecta, and part of the smooth plains (unit Npl). The deposits gradually thin as they extend beyond the depressions. This overflow was likely short lived, because there are few morphologic signatures of shorelines, though we did find a few potential examples (see CTX image P18_007890_1793_XN_00S045W). Previous studies have documented evidence for paleolake overflow on Mars (Coleman and others, 2007; Harrison and Chapman, 2008; Warner and others, 2013b; Marra and others, 2014; Goudge and others, 2019) but none within outflow channel systems. These paleolakes may also have been partially frozen or contained ice at depth (for example, Roda and others, 2014).

This early flooding event may have also begun the incision of Shalbatana Vallis to the north of Orson Welles and Ravi Vallis to the east of Aromatum Chaos (Goudge and others, 2019). This stage of flooding is also mapped to the north of the lower scoured margins of Ravi Vallis (unit AHchle), where model absolute ages from crater counts show the same age as the deposits surrounding the depressions. This portion of the channel had not been mapped previously. It also may have expanded to the south of the lower margins, but we did not observe a contact there so the flood deposits may have been much thinner.

We mapped a small inlet channel leading into Rypin crater that ends in a debris fan (unit AHfa) on the floor of the crater, which we interpret to be a step-type delta (Hauber and others, 2013). Crater statistics for this small unit are not reliable for age dating; however, we assume it formed during the same period as the other potential paleolakes. In addition, we identified layered, light-toned materials in several locations within the chaotic terrain on the floor of Orson Welles crater and within the depressions to the south. Compact Reconnaissance Imaging Spectrometer for Mars (CRISM) analyses of these deposits show evidence for Fe/Mg smectites (Berman and others, 2017). These observations provide further evidence for the presence of paleolakes within the map area.

The temporal relation between flooding and collapse in this region is complex and the exact sequence of events is still unknown, but our observations suggest that there were alternating phases of flooding and collapse. We mapped a large number of depressions, collapse pits, faults, and troughs around Orson Welles crater, particularly to the south and southeast, including the Aromatum Chaos depression, with various depths (from ~1.5 to 3 km), suggesting a sustained phase of subsidence and collapse as groundwater began to evacuate the subsurface beneath weakened crustal materials (Rodriguez and others, 2003, 2005).

Collapse and subsidence of the infill materials in Orson Welles (and potentially Aromatum Chaos) may have begun concurrently with when they were filled with water and continued into the Early Amazonian, forming the chaotic terrain materials (units AHcth and AHctl). We identified two chaotic terrain units, a higher unit and a lower unit (fig. 3). Rotto and Tanaka (1995) had a similar scheme but mapped only the lower unit in Orson Welles crater and the higher unit in Aromatum Chaos and Ravi Valles, whereas we mapped both in each system. Each type of chaotic terrain unit that we mapped has a distinct elevation and morphology and, additionally, has a distinct origin: the higher chaotic terrain materials (unit AHctl) are derived entirely from fill deposits (unit Hf); the lower chaotic terrain materials (unit AHctl) are derived from a combination of fill deposits and collapsed wall materials. The walls of Orson Welles crater have undergone a large degree of collapse and retreat (~40 km at the south margin and ~30 km to the east-northeast) as evidenced by the noncircular shape of the crater and lack of crater rim. Some of these materials were transported downstream. The westernmost chaotic terrain materials in Aromatum Chaos contain larger blocks than those farther downstream and still largely retain the orientation of the wall; these may represent a later stage of wall collapse and retreat.

Other outflow-channel systems that originate from chaotic terrains are different because they do not originate from craters, making this system unique. The chaotic terrains in other regions are hypothesized to have formed from collapsed and subsided plains materials (that may have had high ice contents, for example, Gallagher and others, 2018). In Orson Welles, however, the chaotic terrain must have formed from the collapse of materials that filled the crater, and these materials date to the Hesperian. We mapped the retained mesas of fill materials (unit Hf) within the chaotic terrains to reflect this difference, which was not done in previous maps.

The different morphologies between the two chaotic terrain units reveal that they were eroded by different geologic processes. The lower chaotic-terrain materials (unit AHctl) underwent more fluvial erosion than the higher chaotic-terrain materials (unit AHcth) given that they are smaller and more rounded. This suggests that the lower materials were subject to an increase in discharge. This change in discharge could be continuous from earlier flooding or from a recharged groundwater outburst. The higher discharge event likely led to the narrower and deeper incision of Shalbatana Vallis.

Similarly, in Aromatum Chaos, higher-discharge flood events incised Ravi Vallis to its lower, more constrained levels, which include smooth and etched deposits. The ridges in the etched deposits are indicative of erosion from high-velocity flooding. Eroded materials were likely deposited downstream within Hydraotes Chaos (and likely transported from there to Chryse Planitia). Smooth lower floor deposits (unit AHchls) in Ravi Vallis and Shalbatana Vallis show few fluvial bedforms and indicate later stages of lower discharge flooding after the deeper channels were already incised that may have been dominated by debris that buried bedforms (Rodriguez and others, 2006a,b). Crater counts on outflow channel floors reveal that flooding events throughout Shalbatana and Ravi Valles may have continued into the Early Amazonian.

Fractures in the fill materials of other craters in the map area (unit Hf) likely occurred concurrently with the collapse in Orson Welles and Aromatum Chaos. Sato and others (2010) suggested that these fractures form by groundwater discharge and collapse over subsequent cavities similar to other chaotic terrains, while Roda and others (2014) suggested that they form in subice lakes.

Amazonian Period

During the Amazonian, the map area was subject to continued flooding events and the deposition of flow units and surficial materials. The lobate flow material (unit Alf) was sourced from a fissure or other source vent that was subsequently destroyed during ongoing collapse and retreat of the canyon wall (unit HNu), because we observed no apparent source. The rugged, lobate margins of this deposit, along with observations of thermally bright, boulder-rich ejecta deposits around small craters that superpose the flow, suggest to us that this flow is volcanic in nature. Previous authors have suggested a link between groundwater outbursts and magmatic heating and lava flows in this region (for example, Leverington, 2019b), and our observations provide additional evidence for this.

Collapse and retreat of the wall of Orson Welles crater contributed to the occurrence of landslides (unit Al) around its margins that superpose all of the other deposits on the crater floor, except for the field of dunes (unit Ad) on the southwestern part of the floor. The dunes are stratigraphically the youngest feature in the map area and, with just a few superposed impact craters, could be active in modern geologic time.

References Cited

Adler, J.B., Bell, J.F., Fawdon, P., Davis, J., Warner, N.H., Sefton-Nash, E., and Harrison, T.N., 2018, Hypotheses for the origin of the Hypanis fan-shaped deposit at the edge of the Chryse escarpment, Mars—Is it a delta?: Icarus, v. 319, p. 885–908.

Baker, V.R., 2001, Water and the martian landscape: Nature, v. 412, p. 228–236.

Baker, V.R., and Milton, D.J., 1974, Erosion by catastrophic floods on Mars and Earth: Icarus, v. 23, p. 27–41.

Baker, V.R., Strom, R.G., Gulick, V.C., Kargel, J.S., Komatsu, G., and Kale, V.S., 1991, Ancient oceans, ice sheets, and the hydrological cycle on Mars: Nature, v. 352, p. 589–594.

Berman, D.C., Weitz, C.M., Rodriguez, J.A.P., and Crown, D.A., 2017, Geologic mapping and spectral analyses of the source region of Shalbatana Vallis, Mars: Lunar and Planetary Science Conference 48, abstract 1513.

Cabrol, NA., and Grin, E.A., 1999, Distribution, classification, and ages of Martian impact crater lakes: Icarus, v. 142, p. 160–172.

Cabrol, NA., and Grin, E.A., 2001, The evolution of lacustrine environments on Mars—Is Mars only hydrologically dormant?: Icarus, v. 149, p. 291–328.

Cabrol, N.A., Grin, E.A., and Dawidowicz, G., 1995, Shalbatana Vallis (Mars)—Headwater migration as an alternative to recharge process [abs.]: Lunar and Planetary Science Conference 26, p. 203–204.

Cabrol, N.A., Grin, E.A., and Dawidowicz, G., 1997, A model of outflow generation by hydrothermal underpressure drainage in a volcano-tectonic environment, Shalbatana Vallis (Mars): Icarus, v. 125, p. 455–464.

Carr, M.H., 1979, Formation of Martian flood features by release of water from confined aquifers: Journal of Geophysical Research, v. 84, p. 2995–3007.

Carr, M.H., 1981, The surface of Mars: New Haven, Conn., Yale University Press, 232 p.

Carr, M.H., 1995, The Martian drainage system and the origin of valley networks and fretted channels: Journal of Geophysical Research, v. 100, p. 7479–7507.

Carr, M.H., 1996, Water on Mars: London, Oxford Univ. Press, 229 p.

Carr, M.H., and Malin, M.C., 2000, Meter-scale characteristics of Martian channels and valleys: Icarus v. 146, p. 366–386.

Chapman, M.G., and Kargel, J.S., 1999, Observations at the Mars Pathfinder site—Do they provide "unequivocal" evidence of catastrophic flooding?: Journal of Geophysical Research, v. 104, no. E4, p. 8671–8678.

Clifford, S.M., 1993, A model for the hydrologic and climatic behavior of water on Mars, Journal of Geophysical Research, v. 98, p. 10973–11016.

Clifford, S.M., and Parker, T.J., 2001, The evolution of the martian hydrosphere—Implications for the fate of a primordial ocean and the current state of the northern plains: Icarus v. 154, p. 40–79.

Coleman, N.M., Dinwiddie, C.L., and Baker, V.R., 2007, Evidence that floodwaters filled and overflowed Capri Chasma, Mars: Geophysical Research Letters, v. 34, no. 7, 5 p.

Crumpler, L.S., 1997, Geotraverse from Xanthe Terra to Chryse Planitia,Viking 1 Lander region, Mars: Jounal of Geophysical Research, v. 102, no. E2, p. 4201–4218.

Di Achille, G.L., and Hynek B.M., 2010, Ancient ocean on Mars supported by global distribution of deltas and valleys: Nature Geoscience, v. 3, no. 7, p. 459–463.

Di Achille, G., Marinangeli, L., Ori, G.G., Hauber, E., Gwinner, K., Reiss, D., and Neukum, G., 2006, Geological evolution of the Tyras Vallis paleolacustrine system, Mars: Journal of Geophysical Research, v. 111, no. E04003.

Di Achille, G., Ori, G.G., and Reiss, D., 2007, Evidence for late Hesperian lacustrine activity in Shalbatana Vallis, Mars: Journal of Geophysical Research, v. 112, no. E07007.

Fassett, C. I., and Head, J.W., III, 2008, The timing of Martian valley network activity—Constraints from buffered crater counting: Icarus, v. 195, no. 1, p. 61–89.

Fawdon, P., Gupta, S., Davis, J.M., Warner, N.H., Adler, J.B., Balme, M.R., Bell, J.F., III, Grindrod, P.M., and Sefton-Nash, E., 2018, The Hypanis Valles delta—The last highstand of a sea on early Mars?: Earth and Planetary Science Letters, v. 500, p. 225–241.

Gallagher, C., Balme, M., Soare, R., and Conway, S.J., 2018, Formation and degradation of chaotic terrain in the Galaxias regions of Mars—Implications for near-surface storage of ice: Icarus, v. 309, p. 69–83.

Golombek, M.P., Cook, R.A., Economou, T., Folkner, W.M., Haldemann, A.F.C., Kallemeyn, P.H., Knudsen, J.M., Manning, R.M., Moore, H.J., Parker, T.J., and Rieder, R., 1997, Overview of the Mars Pathfinder mission and assessment of landing site predictions: Science, v. 278, no. 5344, p. 1743–1748.

Goudge, T.A., Fassett, C.I., and Mohrig, D., 2019, Incision of paleolake outlet canyons on Mars from overflow flooding: Geology, v. 47, no. 1, p. 7–10.

Goudge, T.A., Head, J.W., Mustard, J.F., and Fassett, C.I., 2012, An analysis of open-basin lake deposits on Mars—Evidence for the nature of associated lacustrine deposits and post-lacustrine modification processes: Icarus, v. 219, p. 211–229.

Gourronc, M., Bourgeois, O., Mege, D., Pochat, S., Bultel, B., Masse, M., Le Deit, L., Le Mouelic, S., and Mercier, D., 2014, One million cubic kilometers of fossil ice in Valles Marineris—Relicts of a 3.5 Gy old glacial land system along the Martian equator: Geomorphology, v. 204, p. 235–255.

Greeley, R., Theilig, E., Guest, J.E., Carr, M.H., Masursky, H., and Cutts, J.A., 1977, Geology of Chryse Planitia: Journal of Geophysical Research, v. 82, no. 28, p. 4093–4109.

Harrison, K.P., and Chapman, M.G., 2008, Evidence for ponding and catastrophic floods in central Valles Marineris, Mars: Icarus, v. 198, no. 2, p. 351–364.

Hartmann, W.K., 2005, Martian cratering—8. Isochron refinement and the history of martian geologic activity: Icarus, v. 174, p. 294–320.

Hauber, E., Gwinner, K., Kleinhans, M., Reiss, D., Di Achille, G., Ori, G.-G., Scholten F., Marinangeli, L., Jaumann, R., and Neukum, G., 2009, Sedimentary deposits in Xanthe Terra—Implications for the ancient climate on Mars: Planetary and Space Science, v. 57, no. 8–9, p. 944–957.

Hauber, E., Platz, T., Reiss, D., Le Deit, L., Kleinhans, M., Marra, W., de Haas, T., and Carbonneau, P., 2013, Asynchronous formation of Hesperian and Amazonian-aged deltas on Mars and implications for climate: Journal of Geophysical Research, v. 118, p. 1529–1544.

Hopper, J.P., and Leverington, D.W., 2014, Formation of Hrad Vallis (Mars) by low viscosity lava flows: Geomorphology, v. 207, p. 96–113.

Howard, A.D., Moore, J.M., and Irwin, R.P., III, 2005, An intense terminal epoch of widespread fluvial activity on early Mars—1. Valley network incision and associated deposits: Journal of Geophysical Research, v. 110, no. E12S14.

Irwin, R.P., III, Howard, A.D., Craddock, R.A., and Moore, J.M., 2005, An intense terminal epoch of widespread fluvial activity on early Mars—2. Increased runoff and paleolake development: Journal of Geophysical Research, v. 110, no. E12S15, https://doi.org/10.1029/2005JE002460.

Kneissl, T., van Gasselt, S., and Neukum, G., 2011, Map-projection-independent crater size-frequency determination in GIS environments—New software tool for ArcGIS: Planetary Space Science, v. 59, p. 1243–1254.

Leverington, D.W., 2011, A volcanic origin for the outflow channels of Mars—Key evidence and major implications: Geomorphology, v. 132, p. 51–75.

Leverington, D.W., 2019a, Constraints on the nature of the effusive volcanic eruptions that incised Ravi Vallis, Mars: Planetary and Space Science, v. 167, p. 54–70.

Leverington, D.W., 2019b, Formation of Ares Vallis (Mars) by effusions of low-viscosity lava within multiple regions of chaotic terrain: Geomorphology, v. 345, no. 106828.

Lucchitta, B.K., 1982, Ice sculpture in the martian outflow channels: Journal of Geophysical Research, v. 87, p. 9951–9973.

Lucchitta, B.K., 1998, Pathfinder landing site—Alternatives to catastrophic floods and an Antarctic ice-flow analog for outflow channels on Mars: 29th Lunar and Planetary Science Conference, abstract 1287.

Lucchitta, B.K., 2001, Antarctic ice streams and outflow channels on Mars: Geophysical Research Letters, v. 28, p. 403–406.

Lucchitta, B.K., Isbell, N.K., and Howington-Kraus, A., 1994, Topography of Valles Marineris—Implications for erosional and structural history: Journal of Geophysical Research, v. 99, no. E2.

Marra, W.A., Braat, L., Baar, A.W., and Kleinhans, M.G., 2014, Valley formation by groundwater seepage, pressurized groundwater outbursts, and crater-lake overflow in flume experiments with implications for Mars: Icarus, v. 232, p. 97–117.

McCauley, J.F., Carr, M., Cutts, J.A., Hartmann, W.K., Masursky, H., Milton, D.J., Sharp, R.P., and Wilhelms, D.E., 1972, Preliminary Mariner 9 report on the geology of Mars: Icarus, v. 17, no. 2, p. 289–327.

Michael, G.G., 2013, Planetary surface dating from crater size-frequency distribution measurements—Multiple resurfacing episodes and differential isochron fitting: Icarus, v. 226, p. 885–890.

Moore, J.M., and Howard, A.D., 2005, Large alluvial fans on Mars: Journal of Geophysical Research, v. 110, no. E04005.
Nelson, D.M., and Greeley, R., 1999, Geology of Xanthe Terra outflow channels and the Mars Pathfinder landing site: Journal of Geophysical Research, v. 104, no. E4, p. 8653–8669.
Nummedal, D., and Prior, D.B., 1981, Generation of Martian chaos and channels by debris flows: Icarus, v. 45, p. 77–86.
Pacifici, A., 2008, Geomorphological map of Ares Vallis: Bollettino Societa Geologica Italiana (Italian Journal of Geosciences), ASI Planetary Map Series, Map No. 1, v. 127, no. 1, p. 75–92.
Pieri, D., 1976, Distribution of small channels on the Martian surface: Icarus, v. 27, no. 1, p. 25–50.
Roda, M., Kleinhans, M.G., Zegers, T.E., and Oosthoek, J.H.P., 2014, Catastrophic ice lake collapse in Aram Chaos, Mars: Icarus, v. 236, p. 104–121.
Roda, M., Marketos, G., Westerweel, J., and Govers, R., 2017, Morphological expressions of crater infill collapse—Model simulations of Chaotic Terrains on Mars: Geochemistry, Geophysics, Geosystems, v. 18, no. 10, p. 3687–3699.
Rodriguez, J.A.P., Baker, V.R., Liu, T., Zarroca, M., Travis, B., Hui, T., Komatsu, G., Berman, D.C., Linares, R., Sykes, M.V., and Banks, M.E., 2019, The 1997 Mars Pathfinder spacecraft landing site—Spillover deposits from an early Mars inland sea: Scientific Reports, v. 9, no. 1, p. 1–9.
Rodriguez, J.A.P., Gulick, V.C., Baker, V.R., Platz, T., Fairen, A.G., Miyamoto, H., Kargel, J.S., Rice, J.W., and Glines, N., 2014, Evidence for Middle Amazonian catastrophic flooding and glaciation on Mars: Icarus, v. 242, p. 202–210.
Rodriguez, J.A.P., Kargel, J.S., Baker, V.R., Gulick, V.C., Berman, D.C., Fairen, A.G., Linares, R., Zarroca, M., Yan, J., Miyamoto, H., and Glines, N., 2015a, Martian outflow channels—How did their source aquifers form, and why did they drain so rapidly?: Nature Scientific Reports, v. 5, no. 13404, https://doi.org/10.1038/srep13404.
Rodriguez, J.A.P., Kargel, J., Crown, D.A., Bleamaster, L.F., III,, Tanaka, K.L., Baker, V., Miyamoto, H., Dohm, J.M., Sasaki, S., and Komatsu, G., 2006b, Headward growth of chasmata by volatile outbursts, collapse, and drainage—Evidence from Ganges Chaos, Mars: Geophysical Research Letters, v. 33, no. L18203.
Rodriguez, J.A.P, Kargel, J.S., Tanaka, K.L., Crown, D.A., Berman, D.C., Fairén, A.G., Baker, V.R., Furfaro, R., Candelaria, P., and Sasaki, S., 2011, Secondary chaotic terrain formation in the higher outflow channels of southern circum-Chryse, Mars: Icarus, v. 213, p. 150–194.
Rodriguez, J.A.P., Platz, T., Gulick, V., Baker, V.R., Fairen, A.G., Kargel, J., Yan, J., Miyamoto, H., and Glines, N., 2015b, Did the Martian outflow channels mostly form during the Amazonian Period?: Icarus, v. 257, p. 387–395.
Rodriguez, J.A.P., Sasaki, S., Kuzmin, R.O., Dohm, J.M., Tanaka, K.L., Miyamoto, H., Kurita, K., Komatsu, G., Fairen, A.G., and Ferris, J.C., 2005, Outflow channel sources, reactivation, and chaos formation, Xanthe Terra, Mars: Icarus, v. 175, p. 36–57.
Rodriguez, J.A.P., Sasaki, S., and Miyamoto, H., 2003, Nature and hydrological relevance of the Shalbatana complex underground cavernous system: Geophysical Research Letters, v. 30, no. 6, 1304, https://doi.org/10.1029/2002GL016547.
Rodriguez, J.A.P., Tanaka, K.L., Miyamoto, H., and Sasaki, S., 2006a, Nature and characteristics of the flows that carved the Simud and Tiu outflow channels, Mars: Geophysical Research Letters, v. 33, no. L08S04, https://doi.org/10.1029/2005GL024320.
Rotto, S., and Tanaka, K.L., 1995, Geologic/geomorphic map of the Chryse Planitia region of Mars: U.S. Geological Survey Miscellaneous Investigations Series Map I–2441–A, scale 1:5,000,000.
Sato, H., Kurita, K., and Baratoux, D., 2010, The formation of floor-fractured craters in Xanthe Terra: Icarus, v. 207, no. 1, p. 248–264.
Saunders, R.S., 1979, Geologic map of the Margaritifer Sinus quadrangle of Mars: U.S. Geological Survey Miscellaneous Investigations Series Map 1–1144, scale 1:5,000,000.
Scott, D.H., and Carr, M.H., 1978, Geologic map of Mars: U.S. Geological Survey Miscellaneous Investigations Series Map I–1083.
Scott, D.H., and Tanaka, K.L., 1986, Geologic map of the western equatorial region of Mars: U.S. Geological Survey Miscellaneous Investigations Series Map I–1802–A.
Sharp, R.P., 1973, Mars—Fretted and chaotic terrains: Journal of Geophysical Research, v. 78, p. 4073–4083.
Skinner, J.A., Jr., Huff, A.E., Black, S.R., Buban, H.C., Fortezzo, C.M., Gaither, T.A., Hare, T.M., and Hunter, M.A., 2022, Planetary geologic mapping protocol—2022: U.S. Geological Survey Techniques and Methods 11–B13, 28 p., https://doi.org/10.3133/tm11B13.
Squyres, S.W., 1989, Urey prize lecture—Water on Mars: Icarus, v. 79, no. 2, p. 229–288.
Tanaka, K.L., 1986, The stratigraphy of Mars: Journal of Geophysical Research, Solid Earth 91, v. B13, p. E139–E158.
Tanaka, K.L., 1997, Sedimentary history and mass flow structures of Chryse and Acidalia Planitiae, Mars: Journal of Geophysical Research, v. 102, no. E2, p. 4131–4150.
Tanaka, K.L., 1999, Debris-flow origin for the Simud/Tiu deposit on Mars: Journal of Geophysical Research, v. 104, p. 8637–8652.
Tanaka, K.L., Skinner, J.A., Jr., and Hare, T.M., 2005, Geologic map of the northern plains of Mars: U.S. Geological Survey Science Investigations Map 2888, scale 1:15,000,000.
Tanaka, K.L., Skinner, J.A., Dohm, J.M., Irwin, R.P., Kolb, E.J., Fortezzo, C.M., Platz, T., Michael, G.G., and Hare, T.M., 2014, Geologic map of Mars: U.S. Geological Survey Scientific Investigations Map 3292, scale 1:20,000,000.
Warner, N.H., Gupta, S., Kim, J.-R., Lin, S.Y., and Muller, J.P., 2010, Hesperian equatorial thermokarst lakes in Ares Vallis as evidence for transient warm conditions on Mars: Geology, v. 38, p. 71–74.
Warner, N.H., Gupta, S., Kim, J.R., Lin, S.Y., and Muller, J.P., 2013a, Retreat of a giant cataract in a long-lived (3.7–2.6 Ga) martian outflow channel: Geology, v. 38, p. 791–794.
Warner, N.H., Gupta, S., Kim, J.R., Muller, J.P., Le Corre, L., Morley, J., Lin, S.Y., and McGonigle, C., 2011, Constraints on the origin and evolution of Iani Chaos, Mars: Journal of Geophysical Research, v. 116, no. E06003.
Warner, N.H., Sowe, M., Gupta, S., Dumke, A., and Goddard, K., 2013b, Fill and spill of giant lakes in the eastern Valles Marineris region of Mars: Geology, v. 41, p. 675–678.
Werner, S.C., and Tanaka, K.L., 2011, Redefinition of the crater-density and absolute-age boundaries for the chronostratigraphic system of Mars: Icarus, v. 215, p. 603–607.
Wilhelms, D.E., 1976, Geologic map of the Oxia Palus quadrangle of Mars: U.S. Geological Survey Miscellaneous Investigations Series Map I–895, scale 1:5,000,000.